An integrative approach to the facile functional classification of dorsal root ganglion neuronal subclasses

Mario J. Giacobassi[a,1], Lee S. Leavitt[a,1], Shrinivasan Raghuraman[a,1], Rishi Alluri[a,1], Kevin Chase[a], Rocio K. Finol-Urdaneta[b], Heinrich Terlau[c], Russell W. Teichert[a], and Baldomero M. Olivera[a,2]

[a]School of Biological Sciences, University of Utah, Salt Lake City, UT 841120; [b]Illawarra Health and Medical Research Institute, University of Wollongong, Wollongong, NSW 2522, Australia; and [c]Institute of Physiology, Christian Albrechts University Kiel, Kiel 24118, Germany

Contributed by Baldomero M. Olivera, January 7, 2020 (sent for review July 22, 2019; reviewed by Michael Adams and Kurt G. Beam)

Somatosensory neurons have historically been classified by a variety of approaches, including structural, anatomical, and genetic markers; electrophysiological properties; pharmacological sensitivities; and more recently, transcriptional profile differentiation. These methodologies, used separately, have yielded inconsistent classification schemes. Here, we describe phenotypic differences in response to pharmacological agents as measured by changes in cytosolic calcium concentration for the rapid classification of neurons in vitro; further analysis with genetic markers, whole-cell recordings, and single-cell transcriptomics validated these findings in a functional context. Using this general approach, which we refer to as tripartite constellation analysis (TCA), we focused on large-diameter dorsal-root ganglion (L-DRG) neurons with myelinated axons. Divergent responses to the K-channel antagonist, κM-conopeptide RIIIJ (RIIIJ), reliably identified six discrete functional cell classes. In two neuronal subclasses (L1 and L2), block with RIIIJ led to an increase in $[Ca]_i$. Simultaneous electrophysiology and calcium imaging showed that the RIIIJ-elicited increase in $[Ca]_i$ corresponded to different patterns of action potentials (APs), a train of APs in L1 neurons, and sporadic firing in L2 neurons. Genetically labeled mice established that L1 neurons are proprioceptors. The single-cell transcriptomes of L1 and L2 neurons showed that L2 neurons are Aδ–low-threshold mechanoreceptors. RIIIJ effects were replicated by application of the $K_v1.1$ selective antagonist, Dendrotoxin-K, in several L-DRG subclasses (L1, L2, L3, and L5), suggesting the presence of functional $K_v1.1/K_v1.2$ heteromeric channels. Using this approach on other neuronal subclasses should ultimately accelerate the comprehensive classification and characterization of individual somatosensory neuronal subclasses within a mixed population.

DRG neurons | conopeptide | neuronal subclasses | calcium imaging

Somatosensory neurons are specialized for a variety of functions; different cell types respond to different sensory inputs by sending a signal to the central nervous system (CNS) relevant to a particular sensory modality (temperature, touch, pain, proprioception, etc.). Furthermore, broad somatosensory neuronal cell classes (e.g., mechanical) may be further subdivided by the specific somatosensory inputs that they are specialized to detect (e.g., low- vs. high-threshold mechanoreceptors). Unambiguous identification of specific cell types within the somatosensory and other systems will ultimately be necessary to understand the neural circuits underlying nervous system function. Two goals were addressed in this study: to provide easy identification of live neurons belonging to discrete functional cell classes within the dorsal-root ganglion (DRG) and to further our understanding of the membrane macromolecules that underlie the differential functions of these neurons.

We integrate 1) structural markers (e.g., size of cell soma), 2) genetic markers (e.g., fluorescently labeled neurons from reporter mice), 3) pharmacological profiling by calcium imaging, 4) electrophysiology, and 5) single-cell transcriptomics to comprehensively classify and validate sensory neuronal cell types.

As key mediators of inter- and intracellular signaling events in the nervous system, ion channels and G protein-coupled receptor (GPCR) are useful for classifying neuronal cell types. We previously developed constellation pharmacology as a calcium imaging-based method using highly selective pharmacological agents to identify combinations of ion-channel and GPCR subtypes in specific neuronal classes (1–6). Small-diameter DRG neurons often differ in their functional expression of a variety of transient receptor potential (TRP) channels (e.g., TRPV1, TRPA1, and TRPM8). However, these channels are not expressed in myelinated large-diameter dorsal-root ganglion (L-DRG) neurons, which have limited pharmacological differentiators to date.

We hypothesized that all neuronal subclasses are likely to differ in the complement of K_v-channel subtypes that they express. The molecular diversity of functional K_v complexes could contribute to and reflect the divergent physiological roles of different neuronal subclasses. One of our long-term goals is to discover and characterize a robust set of subtype-selective pharmacological tools to differentiate between K-channel subtypes that will enable a more incisive, integrative, and complete taxonomy of neuronal subclasses. In this work, we subdivide L-DRG neurons from adult mice into six subclasses based on genetic markers and the phenotypic

Significance

We have used the cellular response to a conopeptide, a highly selective K-channel blocker κM-RIIIJ, as the initial step in an integrated molecular-, cellular-, and systems-level functional analysis to describe and characterize six discrete subclasses of large-diameter mouse dorsal-root ganglion neurons. Analysis of two of these classes (proprioceptors and Aδ–low-threshold mechanoreceptors) by current-clamp electrophysiology and single-cell transcriptome analysis revealed functional differences between the subclasses based on specific molecular components. This integrated strategy is a potentially powerful tool for investigating individual neuronal cell types in functional context. This study also establishes a general approach for defining which specific ion-channel heteromeric combinations are present in different individual neuronal subtypes.

Author contributions: M.J.G., R.W.T., and B.M.O. designed research; M.J.G., S.R., and R.A. performed research; R.K.F.-U. and H.T. contributed new reagents/analytic tools; M.J.G., L.S.L., S.R., R.A., K.C., and B.M.O. analyzed data; and M.J.G., S.R., K.C., R.K.F.-U., R.W.T., and B.M.O. wrote the paper.

Reviewers: M.A., University of California, Riverside; and K.G.B., University of Colorado Anschutz Medical Campus.

The authors declare no competing interest.

[1]M.J.G., L.S.L., S.R., and R.A. contributed equally to this work.

[2]To whom correspondence may be addressed. Email: olivera@biology.utah.edu.

This article contains supporting information online at https://www.pnas.org/lookup/suppl/doi:10.1073/pnas.1911382117/-/DCSupplemental.

First published February 20, 2020.

calcium responses to a single subtype-selective K-channel antagonist, κM-conopeptide RIIIJ (RIIIJ). This peptide was originally obtained from the venom of *Conus radiatus* (7) and is highly selective for heteromeric K_v complexes that contain K_v1.2 and either K_v1.1 or K_v1.6 subunit (8). In this study, we show that RIIIJ likely blocks K_v1.1/1.2 heteromers in a specific subset of the L-DRG neurons.

Two distinct subclasses of L-DRG neurons respond to the presence of RIIIJ with an increase in $[Ca]_i$ (L1 and L2). These are easily distinguished from one another and all other DRG neurons solely by the unique intracellular calcium profiles evoked by the peptide. Using transgenic mice with labeled proprioceptors in constellation pharmacology, we show that L1 neurons are proprioceptors. This was further verified by single-cell transcriptomic analysis, which identified L2 neurons as Aδ–low-threshold mechanoreceptors (Aδ-LTMRs). With easy experimental access to these two rare neuronal subclasses, a more salient characterization was carried out combining calcium imaging, current-clamp recordings, and single-cell transcriptomics. This approach revealed that the remarkable phenotypic differences uncovered by calcium imaging between the L-DRG classes could be correlated to characteristic patterns of electrical activity and calcium buffering phenomena observed in the two neuronal cell types.

Results

Classification of L-DRG Neurons. Our study focused on large-diameter somatosensory neurons from adult mouse lumbar DRG (L-DRG neurons). These neurons, which are partially defined by their comparatively large cell soma size (>500-μm^2 cross-sectional area), are primarily nonnociceptive neurons with myelinated axons that mediate various modalities of low-threshold mechanosensation or proprioception. In addition, the L-DRG neurons do not bind isolectin B4 (IB4) (Fig. 1*A*) and are insensitive to capsaicin, allyl isothiocyanate (AITC), and menthol, agonists of TRPV1, TRPA1, and TRPM8 channels, respectively. In our analysis of 27,216 DRG neurons using independently prepared cell cultures from 22 mice, 5.5% (1,479) of neurons met our criteria for L-DRG neurons (Fig. 1*B*) and had a cross-sectional area >500 μm^2. The six L-DRG neuronal subclasses encompassed in this study are vastly outnumbered by small-diameter neurons comprising about 94% of DRG neurons in our cultures. These non–L-DRG neurons include various types of nociceptors, thermosensors, and unmyelinated low-threshold mechanoreceptors.

Neuronal Responses to RIIIJ Application: Direct and Indirect Effects. Calcium imaging experiments were performed by periodic depolarization of DRG neurons with increasing extracellular potassium (K^+) concentrations from 5 to 20 mM, eliciting increases in $[Ca]_i$ detected by the change in the fluorescence of the Ca^{2+}-binding dye (Fura2-AM). We refer to an increase in $[Ca]_i$ caused by a pharmacological perturbation as a direct effect (DE) of that compound. When a pharmacological perturbation amplifies the increase in $[Ca]_i$ provoked by 20 mM K^+, we describe it as the compound producing an indirect effect (IDE) on the cell (*Methods* shows the quantification of IDE; Fig. 1*C*, L3 and L5).

Response to RIIIJ Differentiates Six Subclasses of L-DRG Neurons. We subdivided L-DRG neurons into six subclasses by two criteria: 1) expression of calcitonin gene-related peptide (CGRP) as detected by GFP expression in neurons obtained from CGRP-GFP reporter mice (Fig. 1*A*) and 2) the type of effect (DE or IDE) elicited by K_v1.2-selective antagonist, conopeptide κM-RIIIJ. L1 to L4 neurons do not express GFP and thus, are considered

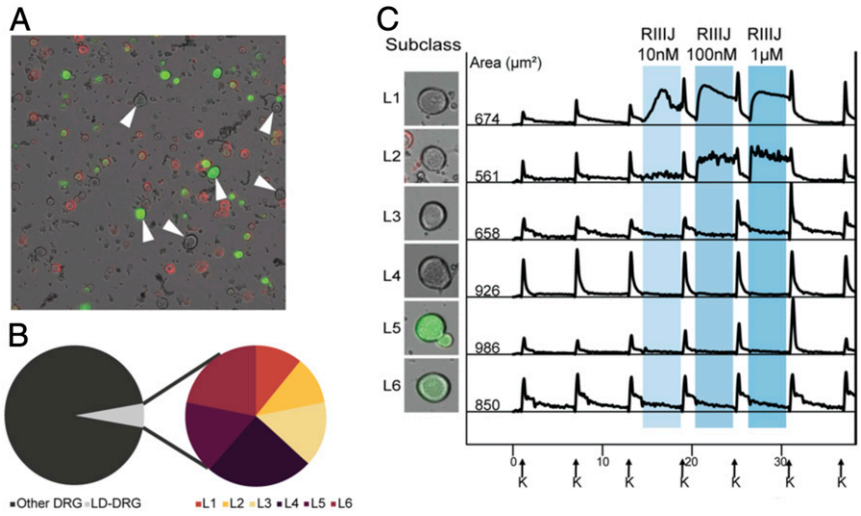

Fig. 1. L-DRG neurons, identified initially by size of cell soma, are subdivided by response to RIIIJ and expression of CGRP. (*A*) Dissociated mouse DRG neurons from CGRP-GFP reporter mice. Bright-field image is overlaid with fluorescent images obtained from IB4 (red) staining and GFP expression (green). IB4 is conjugated to Alexa-Fluor 568 dye (red). The ring staining is indicative of IB4 binding to an extracellular target on the plasma membrane of live cells (nonpeptidergic nociceptors). Soluble GFP is expressed throughout the cytosol of CGRP-expressing neurons (peptidergic nociceptors). Neurons with cross-sectional cell area >500 μm^2 and lacking IB4 stain are reliably identified as L-DRG neurons (indicated by arrows). (*B*) L-DRG neurons make up only 5.5% of the DRG neuronal population. Each subclass of L-DRG neurons makes up between 0.6 and 1.3% of the population. (*C*) L-DRG neurons are subdivided into six subclasses based on the responses to the application of RIIIJ and CGRP-GFP expression. Intracellular calcium profiles (340/380 nm) were obtained from six neurons representative of each group. L1: application of RIIIJ provoked a rise in $[Ca^{2+}]_i$. A smooth rise in $[Ca^{2+}]_i$ is observed that either continues to rise or rises and falls over the course of minutes, sometimes rising more than once. L2: RIIIJ provoked an immediate rise in $[Ca^{2+}]_i$. In contrast to L1, the calcium profiles of these neurons exhibit a "jagged" phenotype that lasts until RIIIJ is removed. Calcium levels stay elevated throughout the RIIIJ incubation but fluctuate between rising and falling several times over a 5-s period. L3: an amplified response (higher peak) to the depolarizing stimulus (high extracellular K^+) following incubation with RIIIJ. L4: no response to the application of RIIIJ during or following the peptide application. L5: expressed CGRP-GFP and responded to RIIIJ similarly to L3 neurons. L6: expressed CGRP-GFP and did not respond to the application of RIIIJ. *Left* shows the bright-field image overlaid with the GFP fluorescence of the neuron from which the data were acquired. Numbers indicate the cross-sectional area of each cell soma in micrometers^2. On the *x* axis (time in minutes), arrows indicate 15-s applications of 20 mM K^+ at 7-min intervals. Shaded areas represent the presence of different concentrations of RIIIJ. On the *y* axis, the ratio of 340/380 nm as a measure of relative intracellular calcium levels is normalized to a scale of zero to one.

CGRP negative, whereas those from L5 and L6 are green in Fig. 1*C*, indicating CGRP expression. Neurons in four of the subclasses (L1 to L3 and L5) responded to RIIIJ with unique DE or IDE. RIIIJ elicited continuous elevation $[Ca]_i$ (smooth DE) in L1 neurons and discontinuous elevation in $[Ca]_i$ (jagged DE) in L2 neurons (Fig. 1*C*). L1 neurons exhibit some cell to cell variability in response to RIIIJ; the $[Ca]_i$ signature always remains "smooth" and typically rises to plateau throughout the RIIIJ incubation. Occasionally, some cells display phenotypic rising and falling more than once during the incubation, but the overall calcium profile remains smooth. $[Ca]_i$ signatures of L2 neurons are very consistent cell to cell; RIIIJ provokes an immediate and sharp spike in $[Ca]_i$ that stays elevated relative to baseline. In contrast to L1, the phenotypic profile rapidly fluctuates between rising and falling phases. The fluctuations are never greater than the initial $[Ca]_i$ influx on RIIIJ application. A detailed description is included in *Methods* for quantification of smooth vs. jagged.

In the remaining L-DRG neuronal subclasses (L3 to L6), RIIIJ did not cause DEs. However, in L3 and L5, the application of RIIIJ produced IDE (Fig. 1*C*). Subclasses L4 and L6 are composed of L-DRG neurons that did not exhibit any obvious changes in $[Ca]_i$ following application of RIIIJ. We summarize the classification scheme for L-DRG neurons in Table 1. Importantly, all six L-DRG neuronal subclasses were present in every cell preparation analyzed (*SI Appendix*, Table S1), and each subclass represented by 0.6 to 1.3% of the total DRG neuronal cell population evaluated (Table 1).

L1 Neurons Are Proprioceptors. Mice, which were injected intraperitoneally (i.p.) with 10 nmol RIIIJ, showed an apparent loss of balance, suggesting reduced proprioception. To investigate whether the L-DRG neuronal subclasses could be correlated with known neuronal cell types, we identified proprioceptors by using DRG neuronal cultures from parvalbumin (PV)-Cre-ER;Ai14 mice. The PV-Cre-ER;Ai14 mice express tdTomato in proprioceptive neurons (*Methods*). Six wells comprising 6,518 total neurons generated from four PV-Cre-ER;Ai14 mice were assessed for sensitivity to RIIIJ by calcium imaging. Evaluation of L-DRG neurons from these mice demonstrated that all neurons classified according to our criteria as L1 expressed the fluorescent protein tdTomato and thus, are recognized as PV-positive proprioceptors ($n = 116$) (*SI Appendix*, Table S2). The experiment shown in Fig. 2 illustrates the distinctive smooth DE elicited by RIIIJ in tdTomato-labeled proprioceptors; 83% of tdTomato-labeled neurons responded with a smooth DE in the presence of RIIIJ.

RIIIJ and Dendrotoxin-K Similarly Affect L-DRG Ca^{2+} Responses. L-DRG neurons express $K_v1.1$ and $K_v1.2$ channels (9). To determine the effects of blocking $K_v1.1$ channel in these neurons, we exposed each neuronal subclass to the $K_v1.1$-selective antagonist Dendrotoxin-K (Dtx-K) (8, 10, 11). Both the smooth DE elicited by RIIIJ in L1 neurons and the jagged DE elicited by RIIIJ in L2 neurons were replicated on application of Dtx-K (Fig. 2). The reversal of DE elicited by 300 nM Dtx-K appeared to be slower than DE caused by 1 μM RIIIJ (Fig. 2, top four traces). Both RIIIJ and Dtx-K elicited IDE in L3 and L5 (Fig. 2). In neuronal subclasses L4 and L6, neither RIIIJ nor Dtx-K produced any observable effects (Fig. 2). The similarities in the DE elicited by RIIIJ and Dtx-K in L1 and L2 neurons and the IDE elicited by both peptides in L3 and L5 neurons suggest that RIIIJ and Dtx-K inhibit the same population of K channels (presumably heteromeric $K_v1.1/1.2$ channels) in these neuronal subclasses.

Affinity to RIIIJ Uncovers Further Diversity of Proprioceptors (L1). The versatility of our approach highlights variability within individual subclasses as illustrated by the graded responses to RIIIJ displayed by L1 DRG neurons. While all L1 neurons defined by smooth RIIIJ-dependent DE also express the proprioceptor reporter (td-tomato), 17% of the PV-positive neurons did not evidence any DE. Further analysis showed that L1 neurons differ in the concentration dependence of their responses to RIIIJ (*SI Appendix*, Fig. S1), which can be used to further subdivide these neurons into high, medium, and low affinity (responsive to 10 nM, 100 nM, or 1 μM RIIIJ, respectively). The most abundant subset (50% of L1 neurons) was the low-affinity responders. The second common subset of L1 neurons was medium-affinity responders (33% of L1 neurons). The least common subset (16% of L1 neurons) was high-affinity responders. Presumably, the td-tomato–labeled neurons that failed to respond to RIIIJ are ultralow-affinity proprioceptors. Two possibilities could account for the td-tomato–labeled neurons that failed to respond to RIIIJ: 1) they are ultralow-affinity proprioceptors, or 2) they are PV-labeled Aβ-rapidly adapting type-I low threshold mechanoreceptors (Aβ-RAI-LTMRs) (Meissner corpuscle afferents), which can express parvalbumin. The graded expression of functional K_v1 channels can be used to characterize a previously indistinguishable population of DRG neurons with the help of selective K-channel ligands as probes. An interesting correlation is that the reversibility of the DE elicited by Dtx-K was slower in the high-affinity L1 neurons (responsive to 10 nM RIIIJ) than in the low-affinity L1 neurons (responsive only to 1 μM RIIIJ) (*SI Appendix*, Fig. S1).

L2 L-DRG Neurons Are Aδ-LTMRs. The conspicuous smooth and jagged DEs elicited by RIIIJ were used to identify and collect L1 and L2 neurons for single-cell RNA sequencing (*Methods*). Comparative transcriptomic analysis of L2 neurons revealed enhanced expression of several established markers of Aδ-LTMRs (Table 2). The presence of genes associated with myelination (Adam22, Nefh, and NRG1) thus verifies that L2 neurons are myelinated. L2 neurons also expressed transcripts encoding for TrkB receptor (*NTRK2*), which is a marker of Aδ-LTMRs (12), and $Ca_v3.2$ (*CACNA1H*), which has been described as a selective marker of Aδ-LTMRs and the unmyelinated C-fiber low-threshold

Table 1. Summary of criteria used to differentiate subclasses of L-DRG neurons

Subclass (% of total neurons)	No. of neurons	RIIIJ				CGRP	
		DE					
		Smooth	Jagged	IDE	No effect	–	+
L1 (0.6)	772	√				√	
L2 (0.6)	919		√			√	
L3 (0.8)	1,114			√		√	
L4 (1.3)	1,140				√	√	
L5 (0.9)	1,427			√			√
L6 (1.2)	1,788				√		√

A total of 27,216 DRG neurons were analyzed, and the number of neurons belonging to each subclass is displayed. √, positive response to the criterion indicated.

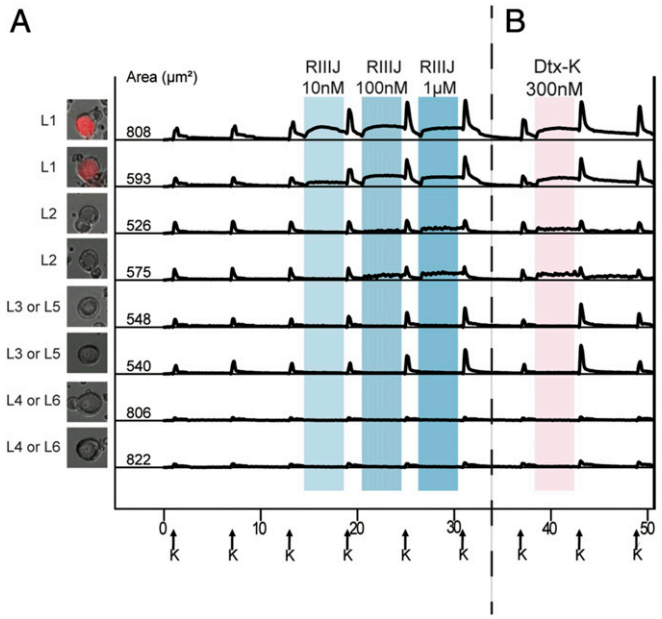

Fig. 2. (*A*) L1 neurons are proprioceptors. (*B*) Dtx-K elicits effects similar to RIIIJ. (*A*) Genetically labeled proprioceptor neurons were identified as L1 neurons by their responses to RIIIJ as observed by calcium imaging. The L1 response phenotype to RIIIJ was exclusively observed in the labeled proprioceptive neurons. L2 to L6 neurons were not proprioceptors as indicated by calcium imaging. Thus, RIIIJ can be reliably used to identify proprioceptive neurons in dissociated culture of mouse DRG neurons. We used PV-IRES-Cre-ER driver mice crossed with Ai14 reporter mice to drive the expression of tdTomato (red) in proprioceptive neurons of the progeny. *Left* shows the bright-field image overlaid with the tdTomato image of the proprioceptor neuron from which the data were acquired. (*B*) Dtx-K elicits effects similar to RIIIJ. In each subclass, the phenotypic calcium response to the application of Dtx-K was similar to the effects elicited by the application of different concentrations of RIIIJ. However, the effects of Dtx-K were often slowly reversible compared with RIIIJ. The column of cell images (*Left*) shows the bright-field image overlaid with the GFP fluorescence of the neuron from which the data are acquired. Numbers indicate the cross-sectional area of each cell soma in micrometers^2. On the *x* axis (time in minutes), arrows indicate 15-s applications of 20 mM K^+ at 7-min intervals. Shaded areas indicate the presence of different concentrations of RIIIJ or Dtx-K. On the *y* axis, the ratio of 340/380 nM as a measure of relative intracellular calcium levels is normalized to a scale of zero to one.

mechanoreceptors (13). All L-DRG neurons analyzed expressed transcripts involved in myelination; however, only L2 neurons expressed transcripts for TrkB and $Ca_v3.2$, strongly suggesting that the jagged DE elicited by RIIIJ (Figs. 2 and 3) can uniquely identify Aδ-LTMRs.

RIIIJ Exposes Distinct Firing Properties in L1 and L2 Neurons. We evaluated L1 and L2 neurons by electrophysiology to investigate the correlation between the $[Ca]_i$ effects elicited by RIIIJ and action potential (AP) firing under whole-cell current clamp. Fig. 3 includes calcium imaging profiles (Fig. 3 *A*, *Upper* and *B*, *Upper*) paired with current-clamp recordings (Fig. 3 *A*, *Lower* and *B*, *Lower*) of L1 (Fig. 3*A*) and L2 (Fig. 3*B*) neurons. In control conditions, the L1 neuron shown in Fig. 3*A* fired a few rapidly adapting APs on current injection of +100 pA (Fig. 3*C*). Strikingly, application of RIIIJ to the same L1 neuron caused it to fire tonically in the absence of any stimulation (0-pA current injection) and responded with regular spiking at frequencies dependent on the input intensity (Fig. 3*A*). Removal of RIIIJ from the bath reduced the firing of this cell from tonic to phasic as observed in control conditions. These results suggest that inhibition of $K_v1.1$/$K_v1.2$ channels causes a profound stimulatory effect on L1 neurons, producing tonic firing and more continuous Ca^{2+} entry reflected by a prolonged and smooth increase in cytosolic calcium concentration.

L2 neurons required stronger stimulation to fire a single AP, which did not become tonic in the presence of RIIIJ. Nevertheless, RIIIJ enhanced AP firing in these neurons in what seemed to be a low-frequency random pattern (Fig. 3*D*). The described firing pattern could account for the jagged DE observed by calcium imaging. The distinct DEs in $[Ca]_i$ caused by RIIIJ in L1 and L2 neurons are consistent with divergent action potential firing patterns in this sensory neuron subclasses.

Simultaneous current-clamp recording and calcium imaging (Fig. 4) in the presence of RIIIJ revealed distinct spike activity that underlies the smooth and jagged DEs of L1 and L2, respectively. Proprioceptors, when incubated in 10 nM RIIIJ, fired a slow train of APs (three to four spikes per second); presenting higher concentrations of RIIIJ resulted in higher spike frequencies. A significant change in $[Ca^{2+}]_i$ was only observed when spike rates were relatively higher (16 spikes per second). In contrast, Aδ-LTMR neurons responded with sparse trains of APs and an almost quantal influx of Ca^{2+} for each spike. These experiments highlight RIIIJ's facile and accessible capacity to functionally differentiate previously unrecognized neuronal subclasses.

Discussion

Future progress in neuroscience will be greatly enhanced by the facile functional identification and characterization of neuronal cell types with specific functions (14). The synergy between calcium imaging, electrophysiology, and single-cell transcriptomics allows for straightforward uncovering of functional differences between patterns of neuronal excitability in response to subtype-selective pharmacological agents. This integration of constellation pharmacology, electrophysiology, and gene expression patterns uncovered by the transcriptomic analysis can be used to correlate the expression profile of ion channels and receptors in distinct neuronal types with observed cell-specific excitability phenotypes. This level of analysis should help to define how the activity of the constellation of receptor and ion-channel isoforms present in a specific neuronal cell type can functionally affect the circuit to which that particular neuron is connected.

We will refer to this general approach as the tripartite constellation analysis (TCA). It combines three technologies (constellation pharmacology, electrophysiology, transcriptomics) to functionally assess and integrate at three biological levels: the physiological system (e.g., proprioception), the specific cellular cell type (e.g., a specific subclass, such as the L1 DRG neurons), and molecular (e.g., a specific ion-channel isoform, such as the $K_v1.2$/$K_v1.1$ heteromer).

In this work, we used a single K channel-targeted ligand (RIIIJ) to functionally distinguish subpopulations of L-DRG neurons through calcium imaging. A major fraction of L-DRG neurons (46%) is not noticeably affected by RIIIJ (e.g., subclasses L4 and L6) (Fig. 2). Another subset of DRG neurons (31%) responds to RIIIJ by amplification of $[Ca]_i$ elicited by subsequent high-K^+ stimulations (e.g., subclasses L3 and L5; IDEs), consistent with RIIIJ modulation of K_v channels that contribute to repolarization of the plasma membrane after a depolarizing stimulus. Finally, a subpopulation of L-DRG neurons (1.2%) displays large increases in $[Ca]_i$ on addition of RIIIJ (DEs; e.g., subclasses L1 and L2), suggesting that RIIIJ-sensitive K_v channels serve as brakes to excitation in these neurons. Consequently, when these are blocked in L1 and L2 neurons, spontaneously firing APs are elicited, ultimately leading to detectable increases in $[Ca]_i$.

The responses of the L-DRG neurons (subclasses L1, L2, L3, and L5) uncovered by pharmacological perturbation with RIIIJ and/or Dtx-K are consistent with the presence of functional K_v channels comprising $K_v1.1$ and $K_v1.2$ subunits. The diversity of phenotypes observed within individual subclasses could be explained

Table 2. Single-cell transcriptomic data from four L1 and four L2 neurons

Gene	Protein encoded	L1	L1	L1	L1	L2	L2	L2	L2
Cacna1h	$Ca_v3.2$	0	0	0	0	2.8	45	319	47
Kcna2	$K_v1.2$	**320**	**301**	**86**	**206**	**223**	**627**	**1,270**	**641**
Kcna1	$K_v1.1$	**609**	**313**	**391**	**184**	**279**	**593**	**981**	**1,115**
Kcnc4	$K_v3.4$	19	0	95	56.8	785	383	562	925
Pvalb	Parvalbumin	**253**	**555**	**257**	**212**	0	0	0	0
Nefh	Neurofilament heavy polypeptide	1,410	1,460	1,111	991	236	312	1,005	826
Ntrk2	Neurotrophic Receptor Tyrosine Kinase 2	0	0	0	1	752	511	1,619	818
Calca	CGRP (α)	1.5	30	3.5	8.6	0	1,080	0	0
Mrgprd	MAS Related GPR Family Member D	0	0	0	0	0	0	0	0
Trpa1	Transient receptor potential ankyrin 1	0	0	0	0	0	0	0	0
Trpm8	Transient receptor potential melastatin 8	0	0	0	0	0	0	0	0
Trpv1	Transient receptor potential vanilloid 1	0	0	0	0	0	0	0	0
Kcna6	$K_v1.6$	1.0	0	56	25	0	4.9	0	1
Adam22	Disintegrin and Metalloproteinase Domain-Containing Protein 22	148	54	133	58	140	254	53	114
Nrg1	Neuregulin 1	80	1,170	229	134	170	74	26	371

Single-cell transcriptomic data from L1 and L2 neurons. Four cells per subclass are tabulated. Counts are reported in transcripts per million. Similarities and diversities in the expression of select genes are displayed. Both L1 and L2 neurons express Kcna1 and Kcna2 (transcripts encoding for Kv1.1 and 1.2), showing the presence of the RIIIJ target. L1 neurons express high levels of Pvalb, which is considered a marker for proprioceptors and is consistent with differential Ca^{2+} buffering in L1 neurons. Adam22, Nefh, and Nrg1 transcripts were detected in both L1 and L2 neurons as myelination markers. Cacna1h and Ntrk2 are expressed in L2 but not L1 neurons, indicating that L2 neurons are Aδ-LTMRs. Mrgprd (indicative of nonpeptidergic nociceptors), Trpa1, Trpm8, and Trpv1 transcripts were not detected in L1 or L2 neurons. Boldface type identifies genes discussed in the text for ease of reading the table and does not denote particular importance.

by the presence of specific complements of K_v-channel isoforms. A recent report by Cordeiro et al. (15) demonstrated that RIIIJ displays higher affinity for heteromeric K_v complexes composed of three $K_v1.2$ subunits and one $K_v1.1$ or $K_v1.6$ subunits ($K_v1.2/1.2/1.2/1.1$ or $K_v1.2/1.2/1.2/1.6$). Therefore, the phenotype of a fraction of the L1 and L2 neurons that respond directly to RIIIJ at the lowest concentration tested (10 nM) and to Dtx-K is consistent with the presence of the high-affinity 3:1 $K_v1.2/K_v1.1$ heteromeric target reported by Cordeiro et al. (15). Furthermore, transcriptomic analysis of individual L1 and L2 DRG neurons revealed abundant expression of Kcna1 and Kcna2 transcripts, encoding $K_v1.1$ and $K_v1.2$, respectively. Kcna6 transcripts ($K_v1.6$), however, were more than two orders of magnitude less abundant (Table 2), making it unlikely that the phenotypic effects of RIIIJ on L1 and L2 DRG neurons are mediated by actions over $K_v1.2/K_v1.6$ heterotetrameric channels.

K_v channels are present in all excitable and secretory cells and have the potential to sculpt subtle differences in function between different neuronal cell types (16). The fine tuning of excitability patterns in diverse neuronal cell types, among other physiological properties, may help to explain the large set (>80) of genes encoding K_v-channel α-subunits in the genomes of mammals (17, 18), with ∼40 of these being different voltage-gated potassium (K_v)-channel subunits. In contrast to other voltage-gated ion channels, functional K_v channels require four α-subunits to form a potassium-selective pore (18). These complexes can comprise four identical α-subunits to form a homotetramer or to form functional heterotetrameric channels (18). Thus, the potential combinatorial complexity of K channels is unprecedented. In this work, we have demonstrated the presence of a heteromeric combination of $K_v1.1$ and $K_v1.2$ subunits in a specific subclass of large DRG neurons.

The assignment of live neurons within a heterogeneous cell population to specific subclasses greatly facilitates their downstream electrophysiological and molecular (i.e., transcriptomic and proteomic) characterization. A demonstration of this integrated approach is the differentiation between L1 and L2 neurons (which together comprise ∼1.2% of all neurons in dissociated mouse DRG cultures). Using genetically labeled mice, we show that L1 neurons are proprioceptors and through single-cell transcriptomics, reveal that L2 neurons are Aδ-LTMRs. Presumably, the unassigned L-DRG subclasses are varieties of Aβ low-threshold mechanoreceptors (Aβ Slowly Adapting 1, Aβ Rapidly Adapting, and Aβ Field low-threshold mechanoreceptors) and myelinated CGRP subclasses (12, 19, 20).

The phenotypic differences uncovered by calcium imaging in response to RIIIJ were correlated with diverse electrical activity assessed by current-clamp electrophysiology. In both L1 and L2 neurons, application of RIIIJ enhanced spontaneous AP firing (Figs. 3 and 4). L1 neurons fired trains of APs with firing rates proportional to the [RIIIJ]. At a low spike rate (approximately three to four APs per second), the registered electrical activity did not cause detectable changes in intracellular calcium. Simultaneous calcium imaging in a current-clamped L1 neuron evidenced detectable $[Ca]_i$ changes only at sufficient spike rates. In contrast, each AP from sporadic, low frequency-firing L2 neurons bathed in RIIIJ could be directly associated with rises in $[Ca]_i$. Differences in gene expression revealed by the single-cell transcriptomic data provide a plausible molecular mechanism as L1 neurons express high levels of parvalbumin, which is a small protein with very high affinity for calcium that buffers free calcium as it enters the cell. Under our experimental conditions, in order to generate a detectable $[Ca]_i$ increase in L1 neurons, it is necessary to overcome the buffering capacity of parvalbumin, which seems to occur when firing rates are greatly enhanced by RIIIJ. Thus, the change in Fura2-bound Ca^{2+} reflects the rate of AP firing in these cells. L2 neurons in contrast to L1 do not express parvalbumin, and therefore, Ca^{2+} increase and AP seem to be temporally correlated.

The essential toolkit for wider dissemination of the TCA strategy comprises a diverse set of highly selective ligands. In this study, the conopeptide RIIIJ serves as proof of principle and founding member. The effect of the peptide on L1 neurons enhances excitability, thus linking a change in the function of a precise signaling macromolecular isoform to a specific cellular phenotype unique to proprioceptive DRG neurons. In turn, this functional phenotype could lead to severe dysfunction of the proprioceptive circuitry, consistent with the symptomatology observed in mice on RIIIJ i.p. injection, which seems to hinder their capacity to maintain normal balance evidenced by repeated falls. We believe that the integrative approach outlined in this study will eventually be

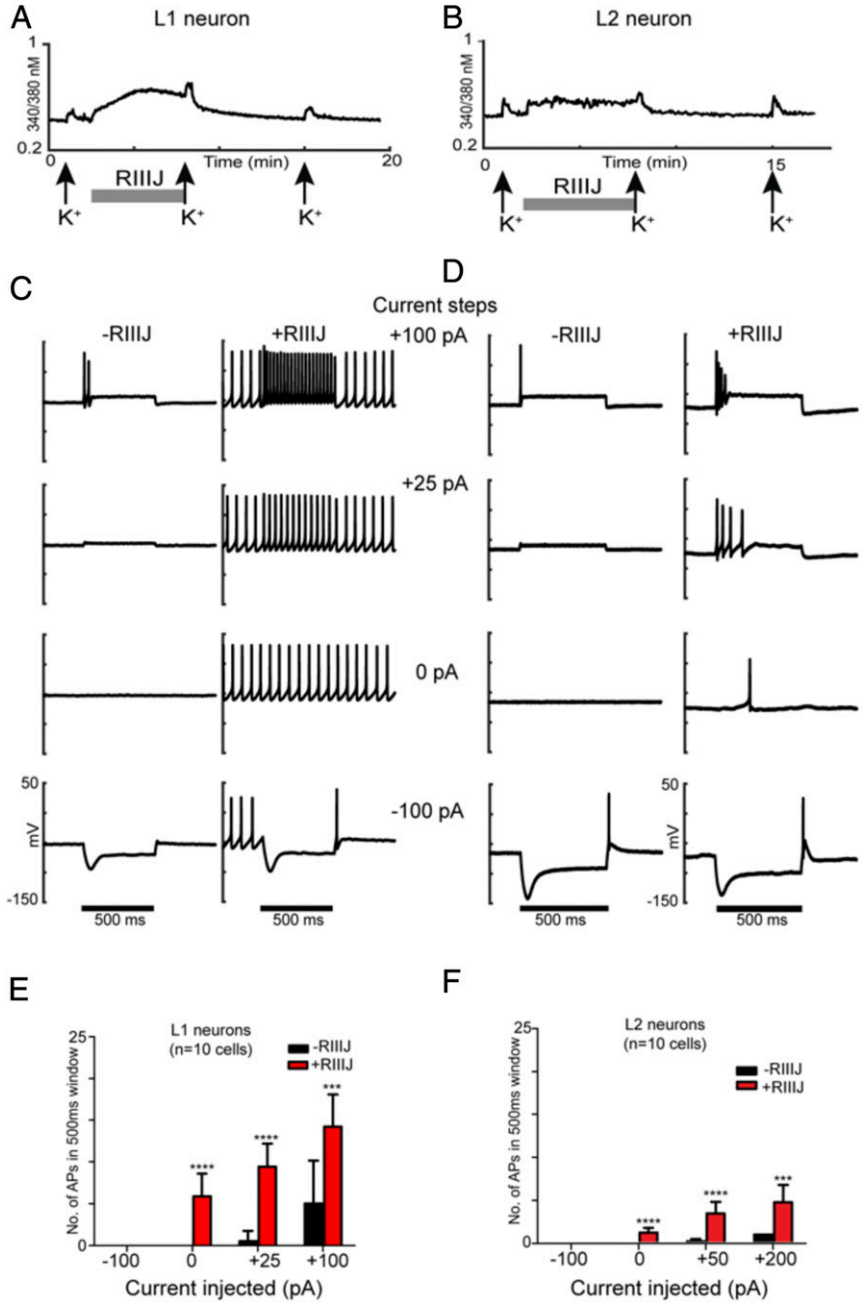

Fig. 3. RIIIJ enhanced firing in L1 and L2 neurons. (*A*) $[Ca^{2+}]_i$ response from an L1 DRG neuron identified by the prototypical smooth DE to the application of RIIIJ. (*B*) $[Ca^{2+}]_i$ response from an L2 neuron identified by its prototypical jagged response to the application of RIIIJ. Three 15-s depolarizing stimuli of 20 mM K^+(indicated by arrows) were applied at 7-min intervals. The application of 1 μM RIIIJ (gray bar) elicited a direct increase in $[Ca^{2+}]_i$ in both L1 and L2 neurons. These two DRG neurons were patched, and electrophysiological recordings were obtained in current-clamp mode. (*C*) Current-clamp recordings from L1 neuron shown in *A*. The membrane potential of the neuron was monitored at a holding current of 0 pA and to current injections −100, 0, +25, and +100 pA in the absence (left traces) and presence (right traces) of 1 μM RIIIJ. RIIIJ induced repetitive APs, and the frequency of firing increased during positive current injections (+25 and +100 pA), while APs were totally suppressed during a −100-pA injection. (*D*) Current-clamp recordings from L2 neuron shown in *B*. The membrane potential of the L2 neuron was monitored at a holding current of 0 pA and to current injections −100, 0, +25, and +100 pA in the absence (left traces) and presence (right traces) of 1 μM RIIIJ. In both neurons, the frequency of firing increased significantly with the increase in positive current injections (+25- and +100-pA steps) in the presence of RIIIJ. In contrast to L1 neurons, L2 neurons did not display tonic firing at 0 pA and displayed a small difference in the number of APs with increase in current injections (no significant difference between +50 and +200 pA). These observations are quantified in *E* and *F* for L1 and L2 neurons, respectively. Black bars represent a 500-ms duration when current steps were applied. The *y* axis represents membrane potential (scale ranges from −150 to +50 mV for all traces). $n = 10$ cells in each group. ***$P < 0.005$ as determined by two-way ANOVA test on Graphpad Prism; ****$P < 0.0001$ as determined by two-way ANOVA test on Graphpad Prism.

useful for obtaining a comprehensive and definitive classification scheme for DRG neurons and will ultimately have the same utility for neuronal cell populations in the brain and across species.

Methods

Transgenic Mice. All procedures in this investigation were approved by the Institutional Animal Care and Use Committee of the University of Utah. Two

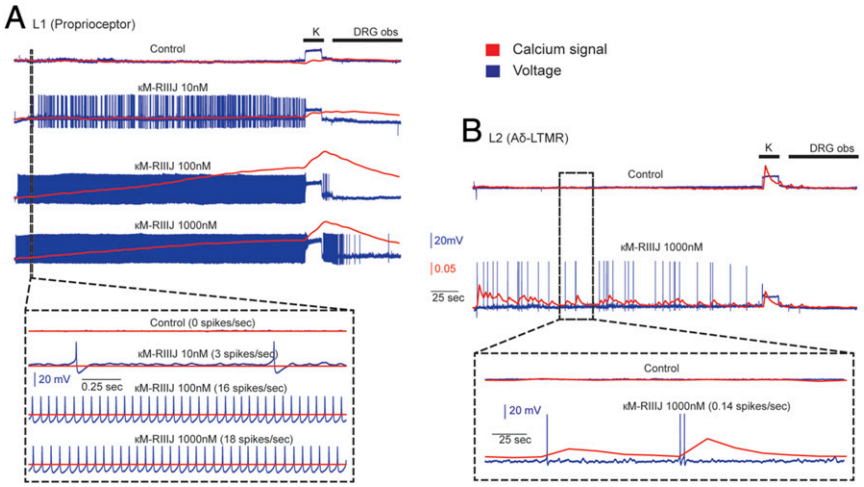

Fig. 4. Simultaneous calcium imaging and intracellular recording. (*A*) L1 neurons (proprioceptors) respond to κM-RIIIJ with a train of APs. At 10 nM, κM-RIIIJ induced a sparse spike train and did not result in a robust calcium signal; higher concentrations of the drug resulted in increases in spike rate, decreases in first spike latency, and a smooth continuous rise in calcium signal. (*B*) L2 Aδ-LTMRs showed sparse bursts of APs and a lower spike rate than proprioceptors. Unlike proprioceptors, calcium signal in response to the drug-induced APs was jagged; each spike resulted in an almost quantal influx of calcium, and multiple spikes in short intervals resulted in summation of calcium influx. DRG obs, DRG observation solution.

strains of transgenic reporter mice were used for identification of specific somatosensory neuronal subclasses: CGRP-GFP mice and PV-ires-Cre;Ai14 reporter mice. CGRP-GFP mice [strain name: STOCK Tg(Calca-EGFP) FG104Gsat/Mmucd] were created by the Gensat project as previously described (21). In this mouse strain, GFP expression is driven by the gene-regulatory elements of CGRP, which primarily labels peptidergic nociceptors in the somatosensory neuronal cell population. We crossed PV-IRES-Cre-ER driver mice (Jackson Laboratory stock #008069) with Ai14 reporter mice (Jackson Laboratory stock #007908) to drive the expression of tdTomato in proprioceptive neurons in the progeny. All of these mice were provided by laboratory of David Ginty, Harvard University, Cambridge, MA.

Constellation Pharmacology. Experiments were performed as described previously (1–6, 22) and detailed in *SI Appendix, Materials and Methods*. Briefly, lumbar DRG neurons from CGRP-GFP mice (in a CD1 genetic background) from ages postnatal (P)41 to P89 were dissociated by treating DRGs with trypsin followed by mechanical trituration and plated on polylysine-coated coverslips. The plated cells were placed in a 5% CO_2 incubator at 37 °C overnight in neuronal culture medium. Cells were incubated with Fura2-AM dye for 1 h at 37 °C before calcium imaging experiments. Pharmacological challenges present in each experiment include AITC at 100 μM, menthol at 400 μM, capsaicin at 300 nM, K^+ at 20 and 40 mM, and RIIIJ at 1 μM. Dtx-K was used at 300 nM. Following the calcium imaging experiments, cells were incubated with Alexa-Flour 568 IB4 to identify IB4-positive nonpeptidergic nociceptors.

For determining DEs, we estimate the noise about a smooth curve over a given interval as $J = sd(y - y_{loe})/\text{mean}(y)$, where y is the raw 340/380 points across the interval of interest and y_{loe} is the smooth curve fit estimated at each time point using loess (23) to predict y based on the time sampling points with a span of 15 points (~30 s). The jitter score is estimated as the ratio of J for the RIIIJ interval and the mean of J for three to five control intervals of the same length. In each experiment, L2 cells have larger jitter scores than L1 cells. The distribution of jitter scores is bimodal, with the low peak representing the L1 cells and the high peak representing the L2 cells. Values <0.5 correspond to the smooth rise phenotype, while values in the range from 0.5 to 2.0 correspond to the jagged phenotype. In experiments with labeled proprioceptor cells (PV-Cre), division of the response phenotypes by this value correctly identified 90% ($n = 72$ proprioceptors from five different mice) of the PV-Cre–labeled cells.

IDEs were estimated as $IDE = (K_{max2} - K_{max1})/(K_{max2} + K_{max1})$, where K_{max1} is the maximum 340/380 ratio within the window of K^+ application before incubation with the compound of interest and K_{max2} is the maximum 340/380 ratio within the window of K^+ application after incubation with the compound of interest. Using control experiments, we determined that 95% of nontreated neurons gave IDE values less than 0.092, which corresponds to an ~20% increase in response maximum. Traces with no DE that exceeded this threshold were scored as amplified (IDE).

Electrophysiological Recordings from Cultured DRG Neurons. Whole-cell current-clamp experiments were performed in tandem and simultaneously with calcium imaging. For tandem recordings, the intracellular pipette solution contained 140 mM potassium aspartate, 13.5 mM NaCl, 1.8 mM $MgCl_2$, 0.09 mM ethylene glycol-bis(beta-aminoethyl ether)-N,N,N′,N′-tetraacetic acid (EGTA), 9 mM 4-(2-hydroxyethyl)-1-piperazineethanesulfonic acid (HEPES), 14 mM creatine phosphate, 4 mM Mg-adenosine triphosphate (ATP), and 0.3 mM Tris guanosine triphosphate (GTP). The pH of the solution was adjusted to 7.2 with KOH, and the osmolarity was adjusted to 290 to 300 milliosmole (mOsM) with glucose. The extracellular bath solution was the same as the DRG observation solution used for calcium imaging experiments and contained 145 mM NaCl, 5 mM KCl, 2 mM $CaCl_2$, 1 mM $MgCl_2$, 1 mM Na-Citrate, 10 mM Hepes, and 10 mM glucose. The pH of extracellular solution was adjusted to 7.4 with NaOH, and the osmolarity was adjusted to 310 to 320 mOsM with glucose. The pipette resistance ranged from 3 to 5 MΩ. Cells with stable resting membrane potential below −40 mV were used for recordings, which were made with a MultiClamp 700 A amplifier and acquired with a DigiData 1440 digitizer. The amplifier and digitizer were controlled by MultiClamp Commander and Clampex10.6, respectively (Molecular Devices). All experiments were done at room temperature (22 °C).

Simultaneous Ca^{2+} Imaging and Current Clamp. ***Electrode construction.*** Patch pipettes were constructed from high-borate borosilicate capillary glass (WPI #1B150-4, 1.5-mm outer diameter, 0.8-mm inner diameter) using a Flaming/Brown-type puller (model P-97; Sutter Instruments). These pipettes had outside tip diameters of ~0.9 to 1.3 μm. Electrode tips are back filled with a solution (pH 7.4) consisting of 2 mM NaCl, 125 mM KCl, 2 mM $MgCl_2$-$6H_2O$, 10 mM Hepes, and glucose at a concentration to bring the final osmolarity to ~290 to 300 mOsmol. These pipettes had resistances between 10 and 25 MΩ. ***Whole-cell recording.*** Individual cells were approached by a patch electrode using a three-axis Microdrive (MPC-200) while maintaining positive pressure and applying −1-nA square-wave pulses(2 Hz) via Multiclamp 700 A (Axon Instruments) to monitor resistance. Cell contact was monitored both under the microscope in bright field and via a small increase in the voltage change; on contact, negative pressure was applied to the pipette to increase the resistance of the seal to gigaohm levels (~1.5 GΩ) (24). After the seal resistance had increased, we started measuring calcium influx using the ratio of bound to unbound Fura2. Either a sinewave current of ±1 nA or negative pressure was used to rupture the patch and gain electrical access to the intracellular membrane potential. Digidata 1440A (Axon CNS) was used to acquire membrane potential and injected current in separate channels at a sampling rate of 10 kHz each. The resistance and capacitance of neuronal membrane were measured by injecting an occasional current pulse of −0.1 nA and fitting a double exponential to differentiate between potential drop across pipette and cell (25).

Single-Cell Transcriptomics. After constellation pharmacology experiments were performed, individual cells were picked using fire-polished glass pipettes with optimized diameter. Cells were lysed, and messenger ribonucleic acid (mRNA) was reverse transcribed to generate complementary DNA (cDNA), which then underwent whole-transcriptome amplification, all using the QIAseq FX Single Cell RNA library kit according to the manufacturer's standard protocol (Qiagen Sciences). The amplified cDNA was used to construct a sequencing library for the Illumina NGS platform also using the QIAseq FX Single Cell RNA library kit. The amplified cDNA was fragmented to 300 bp in size and treated for end repair and A addition followed by adapter ligation and then, cleanup with Agencourt AMPure XP magnetic beads (Beckman Coulter Life Sciences). The cDNA library was submitted to the HCI high-throughput genomics core facility (High Throughput Genomics Shared Resource) for library quality control and sequencing. Sequencing data were analyzed using in-house R scripts described in *SI Appendix, Materials and Methods*.

Data Availability Statement. Data relevant to this work are included in the main text and *SI Appendix*.

ACKNOWLEDGMENTS. This work was supported by Department of Defense Grant PR 161686 "Novel strategies for accelerating non-opioid drug discovery" and National Institute of General Medical Sciences Grant GM 48677 "*Conus* Peptides and Their Receptor Targets: Towards Constellation Pharmacology" (to B.M.O.). We thank Prof. David Ginty for helpful discussions in the preparation of the manuscript and for the gift of transgenic mice used in this study.

1. R. W. Teichert *et al*., Characterization of two neuronal subclasses through constellation pharmacology. *Proc. Natl. Acad. Sci. U.S.A.* **109**, 12758–12763 (2012).
2. S. Raghuraman *et al*., Defining modulatory inputs into CNS neuronal subclasses by functional pharmacological profiling. *Proc. Natl. Acad. Sci. U.S.A.* **111**, 6449–6454 (2014).
3. K. J. Curtice *et al*., Classifying neuronal subclasses of the cerebellum through constellation pharmacology. *J. Neurophysiol.* **115**, 1031–1042 (2016).
4. R. W. Teichert, E.W. Schmidt, B.M. Olivera, Constellation pharmacology: A new paradigm for drug discovery. *Ann. Rev. Pharmacol. and Toxicol.* **55**, 573–589 (2015).
5. R. W. Teichert, T. Memon, J. W. Aman, B. M. Olivera, Using constellation pharmacology to define comprehensively a somatosensory neuronal subclass. *Proc. Natl. Acad. Sci. U.S.A.* **111**, 2319–2324 (2014).
6. R. W. Teichert *et al*., Functional profiling of neurons through cellular neuropharmacology. *Proc. Natl. Acad. Sci. U.S.A.* **109**, 1388–1395 (2012).
7. P. Chen, A. Dendorfer, R. K. Finol-Urdaneta, H. Terlau, B. M. Olivera, Biochemical characterization of kappaM-RIIIJ, a Kv1.2 channel blocker: Evaluation of cardioprotective effects of kappaM-conotoxins. *J. Biol. Chem.* **285**, 14882–14889 (2010).
8. F. C. Wang *et al*., Identification of residues in dendrotoxin K responsible for its discrimination between neuronal K+ channels containing Kv1.1 and 1.2 alpha subunits. *Eur. J. Biochem.* **263**, 222–229 (1999).
9. M. N. Rasband *et al*., Distinct potassium channels on pain-sensing neurons. *Proc. Natl. Acad. Sci. U.S.A.* **98**, 13373–13378 (2001).
10. B. Robertson, D. Owen, J. Stow, C. Butler, C. Newland, Novel effects of dendrotoxin homologues on subtypes of mammalian Kv1 potassium channels expressed in Xenopus oocytes. *FEBS Lett.* **383**, 26–30 (1996).
11. M. V. Sokolov, O. Shamotienko, S. N. Dhochartaigh, J. T. Sack, J. O. Dolly, Concatemers of brain Kv1 channel alpha subunits that give similar K+ currents yield pharmacologically distinguishable heteromers. *Neuropharmacology* **53**, 272–282 (2007).
12. M. Rutlin *et al*., The cellular and molecular basis of direction selectivity of Aδ-LTMRs. *Cell* **159**, 1640–1651 (2014).
13. A. Francois *et al*., The low-threshold calcium channel CaV3.2 determines low-threshold mechanoreceptor function. *Cell Rep.* **10**, 370–382 (2015).
14. H. Zeng, J. R. Sanes, Neuronal cell-type classification: Challenges, opportunities and the path forward. *Nat. Rev. Neurosci.* **18**, 530–546 (2017).
15. S. Cordeiro *et al*., Conotoxin κM-RIIIJ, a tool targeting asymmetric heteromeric Kv1 channels. *Proc. Natl. Acad. Sci. U.S.A.* **116**, 1059–1064 (2018).
16. J. F. Storm, "Potassium currents in hippocampal pyramidal cells" in *Understanding the Brain through the Hippocampus: The Hippocampal Region as a Model for Studying Brain Structure and Function*, J. Storm-Mathisen, J. Zimmer, O. P. Ottersen, Eds. (Progress in Brain Research, Elsevier, New York, NY, 1990), vol. 83, pp. 161–187.
17. L. Y. Jan, Y. N. Jan, Voltage-gated potassium channels and the diversity of electrical signalling. *J. Physiol.* **590**, 2591–2599 (2012).
18. G. A. Gutman *et al*., International Union of Pharmacology. LIII. Nomenclature and molecular relationships of voltage-gated potassium channels. *Pharmacol. Rev.* **57**, 473–508 (2005).
19. L. Li *et al*., The functional organization of cutaneous low-threshold mechanosensory neurons. *Cell* **147**, 1615–1627 (2011).
20. A. Zimmerman, L. Bai, D. D. Ginty, The gentle touch receptors of mammalian skin. *Science* **346**, 950–954 (2014).
21. S. Gong *et al*., A gene expression atlas of the central nervous system based on bacterial artificial chromosomes. *Nature* **425**, 917–925 (2003).
22. T. Memon, K. Chase, L. S. Leavitt, B. M. Olivera, R. W. Teichert, TRPA1 expression levels and excitability brake by K_V channels influence cold sensitivity of TRPA1-expressing neurons. *Neuroscience* **353**, 76–86 (2017).
23. W. S. Cleveland, E. Grosse, W. M. Shyu, "Local regression models" in *Statistical Models in S*, J. M. Chambers, T. J. Hastie, Eds. (Chapman & Hall/CRC, Boca Raton, FL, 1992), chap. 8, pp. 309–376.
24. G. J. Rose *et al*., Combining pharmacology and whole-cell patch recording from CNS neurons, in vivo. *J. Neurosci. Methods* **213**, 99–104 (2013).
25. R. K. Alluri *et al*., Phasic, suprathreshold excitation and sustained inhibition underlie neuronal selectivity for short-duration sounds. *Proc. Natl. Acad. Sci. U.S.A.* **113**, E1927–E1935 (2016).